Wireless Communication of Radio Waves Carrying Orbital Angular Momentum (OAM) Above an Infinite Ground Plane

Wireless Communication of Radio Waves Carrying Orbital Angular Momentum (OAM) Above an Infinite Ground Plane

Lei Wang, *Senior Member, IEEE*, Woocheon Park, Cheng Yang, *Member, IEEE*, Heinz-Dietrich Brüns, Dong Gun Kam, *Senior Member, IEEE*, and Christian Schuster, *Senior Member, IEEE*

***Abstract*—Radio waves carrying orbital angular momentum (OAM) have been intensively studied in recent years with respect to generation, propagation, and communication. In this article, the effect of an infinite ground on OAM wave propagation and communication is investigated numerically using the method of moments (MoM). A circular array of half-wavelength dipoles is taken as a uniform circular array, for the generation and reception of OAM waves. First, electromagnetic image theory is adopted for analysis and numerical investigation of image OAM arrays and their influence of reflections from the ground plane. Employing MoM and mixed-mode scattering parameters, the impact of the ground plane on wireless communication is further explored by varying the communication distances between the transmitting and receiving arrays, heights of OAM arrays above the ground, and array orientations. Compared to OAM-based communication in free space, the effect of the ground plane turns out to be considerable. Specifically, it was found that OAM-based communication not only suffers from destructive influence due to reflections from the ground but also from reduced mode isolation. The results obtained in this article will be fundamental for optimizing OAM-based communication in a realistic environment.**

***Index Terms*—Array antennas, infinite ground plane, method of moments (MoM), orbital angular momentum (OAM), radio waves, wireless communication.**

I. Introduction

IT IS well known that electromagnetic (EM) waves can carry both linear momentum and angular momentum [1], [2]. EM angular momentum consists of spin angular momentum and orbital angular momentum (OAM). In optics, OAM waves are characterized by a phase distribution perpendicular to the beam axis that varies linearly with the angle taken around the beam axis. As a consequence of this phase distribution, the beam axis shows no fields and the wave front becomes a helix in space. Hence, OAM carrying beams are often referred to as vortex, spiral, twist, or helix waves.

In the recent past, it has been proposed that the OAM property of EM waves can be used to boost data rates using light beams carrying OAM for transmitting information in free-space optical systems [2]–[5]. Dipole arrays have been introduced to generate and detect OAM in radio waves [6]–[9], proving that OAM can also be used in the low-frequency radio domain and is not restricted to the optical frequency range. The selection and configuration of radiators were carefully checked with regard to the symmetry breaking [10] and OAM density distributions [11]. An OAM radio system was studied in 2010 [12] and it was found that an OAM antenna array generates a rotation in the phase front also in radio beams. The OAM-based radio communication was investigated with regard to the difference with traditional multiple-input-multiple-output (MIMO) communication methods [13], [14]. The comparison to MIMO also was done in a highly reverberant environment and showed that the OAM multiplexing exhibits comparable performance [15]. Optimization [16] and application [17] of the OAM radio communication system were carried on. A comparison between the classic antenna gain and link budget was carried out in [18]. The link budget concept was introduced for OAM communication link in [19]. Refracted and reflected OAM waves from a dielectric slab were theoretically analyzed and tested with respect to electric fields in [20]. Nevertheless, most of the OAM studies published so far are for OAM antennas in a homogeneous medium, such as in free space. However, antennas are usually operated in the presence of other structures, e.g., dielectric and metallic objects and structures, that influence the wireless communication between OAM wave transmitters and receivers. For instance, whether one OAM mode transmitted from a Tx array can be distinguished at an Rx array in the presence of other objects like a ground plane has not been fully clarified yet.

A ground plane in its ideal form is infinite in extent and perfectly conducting, usually referred to as a perfect ground plane. In this article, effects of a perfect ground plane on OAM waves and wireless communication will be investigated in a numerical manner. The basic setup is illustrated in Fig. 1. Several aspects will be explored: existence and orientation of image OAM arrays, EM field distributions, and OAM communication [21]–[23] versus communication distances and heights above the ground plane. We believe the investigation in this

Manuscript received October 21, 2019; revised December 17, 2019; accepted December 23, 2019. *(Corresponding author: Lei Wang.)*

L. Wang, C. Yang, H.-D. Brüns, and C. Schuster are with the Institute of Electromagnetic Theory, Hamburg University of Technology, 21079 Hamburg, Germany (e-mail: lei.wang@tuhh.de; cheng.yang@tuhh.de; bruens@tuhh.de; schuster@tuhh.de).

W. Park is with the Electronics and Telecommunications Research Institute, Daejeon 34129, South Korea (e-mail: wpark@etri.re.kr).

D. G. Kam is with the Department of Electrical and Computer Engineering, Ajou University, Suwon 16499, South Korea (e-mail: kam@ajou.ac.kr).

Color versions of one or more of the figures in this article are available online at https://ieeexplore.ieee.org.

Digital Object Identifier 10.1109/TEMC.2020.2965656

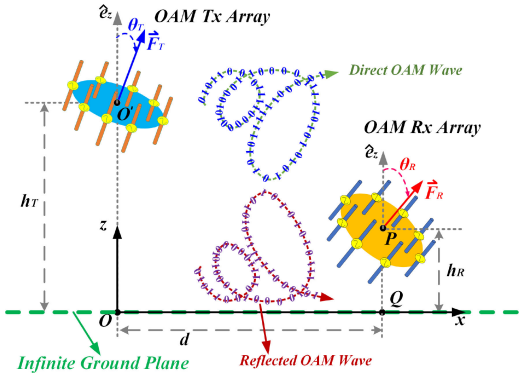

Fig. 1. Illustration of wireless communication between OAM-based antenna arrays above an infinite ground plane (xy-plane), where d is the horizontal distance between the transmitting (Tx) and receiving (Rx) arrays, and h_T and h_R are the heights above the infinite ground. The polar angles θ_T and θ_R are the orientation angles of the Tx and Rx arrays, respectively, and the normal vectors $\vec{F}_T$ and $\vec{F}_R$ are defined with respect to the centers of each dipole array, respectively.

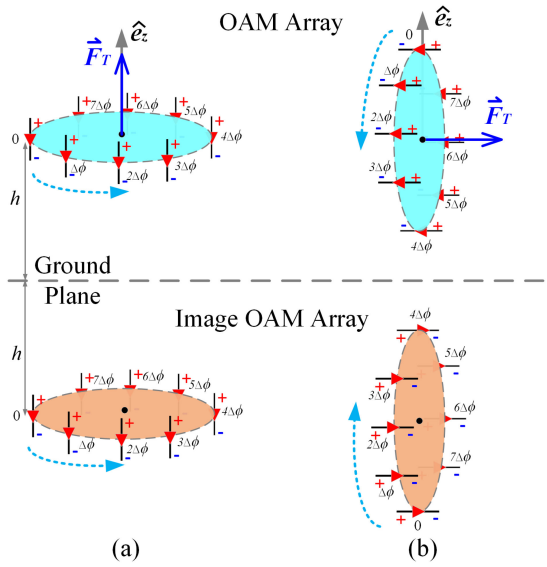

Fig. 2. Illustration of EM image theory applied to OAM arrays above an infinite ground plane. Referring to Fig. 1, the transmitting array Tx is taken as example with (a) $\theta_T = 0°$, and (b) $\theta_T = 90°$.

article is important for EM compatibility engineering, as the ground effect on antennas and wireless communication are common causes for interference in realistic applications.

The remainder of this article is structured as follows. In Section II, image OAM arrays are studied using EM image theory and the ground effects on EM fields are explored numerically. In Section III, the effect of varying distances and heights above the ground on the OAM mode communication between two OAM arrays is studied, including the effect of fading with distance. Finally, in Section IV, the conclusion with respect to realistic OAM-based communication above an infinite ground plane is drawn.

II. Image OAM Arrays and EM Fields

Considering the variation of an antenna above a perfect ground plane, the interaction between the antenna and the ground can be well explained and predicted by using EM image theory [24]. By applying EM image theory, image antennas or arrays can be used to replace the infinite ground plane, thus eliminating the need for its modeling. In the following subsections, EM image theory is adopted and extended to an OAM array. Then, the numerical implementation of the image theory is described, by means of which EM fields for $z > 0$ (see Fig. 1) can be accurately computed.

A. Image OAM Arrays

In this section, a uniform circular array composed of ideal half-wavelength dipoles is used as a transmitter of OAM waves, as illustrated in Fig. 1. The linear dipoles are oriented along the circular array axis to achieve good OAM symmetry [10]. A unit vector $\vec{F}_T$ is introduced to indicate the orientation of a transmitting OAM array. The direction of $\vec{F}_T$ is defined according to a right-hand rule: right fingers curled toward increasing phase offset (from 0, $\Delta\phi$, $2\Delta\phi$, $3\Delta\phi$, ...) will lead to the right thumb pointing in the direction of $\vec{F}_T$.

Applying EM image theory [24] to each dipole in the original OAM transmitting array Tx, an image OAM array T′x is obtained, as illustrated in Fig. 2. It is found that when $\vec{F}_T$ is perpendicular to the ground, the direction of increasing phase on the image array remains the same as the original one. However, when $\vec{F}_T$ is parallel to the ground, as shown in Fig. 2(b), the direction of the increasing phase is opposite to the original one. The configurations of Fig. 2 are in that regard extreme cases of a continuum of array configurations above ground. Our article will focus on these two.

In conclusion, the structure of the image OAM array is mirrored from the original OAM array with the same distance to the infinite ground plane. The current direction on each antenna element and the increasing phase direction of the OAM array are both dependent on the array orientation, leading to a complicated behavior of interference above the ground plane.

B. Numerical Implementation of Image OAM Arrays

In order to compute the field propagation of OAM waves and investigate the transmission of OAM modes quantitatively, a frequency-domain full-wave simulator has been applied, which has the ability to include a perfect ground plane. Specifically, based on the method of moments (MoM), the modeling of an infinite ground plane can be carried out by adding an additional term to each element of the original system matrix. This term is related to the corresponding image current basis function [25], [26]. As a result, the implementation of EM image theory doubles the effect for the computation of the system matrix but will not increase the cost for solving the system of equations as the order of the system matrix is not increased compared with the case of a nonexistent ground plane. The MoM solver provided by[25] is utilized for all the simulations throughout this article.

C. EM Fields of OAM Arrays

In this section, the influence of the infinite ground will be analyzed from the perspective of EM field distributions. For

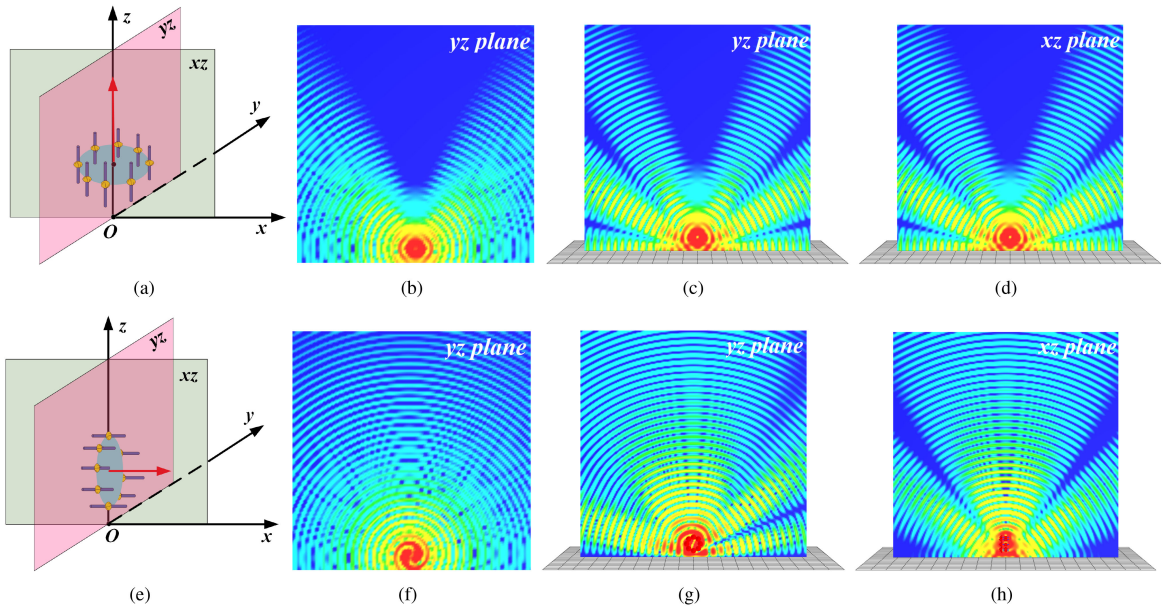

Fig. 3. Electric field distribution of OAM mode 1 in an observation window (50×50 m^2) at $x = 0$ m. The OAM T_x array is located at $h_T = 3$ m above the infinite ground plane. (a)–(d) are cases when $\theta_T = 0^\circ$, whereas (e)–(h) are cases when $\theta_T = 90^\circ$. Plotting scale is -10 to -40 dBV/m. (b) and (f) yz-plane in free space without an existing ground plane. (c) and (g) yz-plane above an existing ground plane. (d) and (h) xz-plane above an existing ground plane.

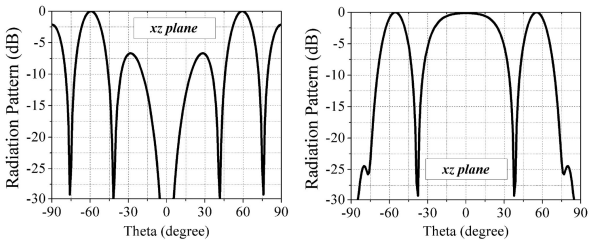

Fig. 4. Normalized radiation patterns in xz-plane versus θ, (a) is the case when $\theta_T = 0^\circ$, whereas (b) is the case when $\theta_T = 90^\circ$.

the generation of OAM waves, a circular array consisting of eight dipoles is used as a transmitting array. The diameter and the length of each dipole are 0.1 mm and 1.38 m, respectively, realizing ideal dipoles to radiate at 100 MHz with an input scattering parameter $|S_{11}|$ of -12.7 dB. The corresponding wavelength is ≈ 2.998 m. The diameter of the array circle is 3.0 m. As an example, an OAM wave of mode 1 [21] is excited by dipoles feeding with uniform amplitude and a phase offset $\Delta\phi = 45^\circ$.

In the case, when the Tx array is vertically oriented, i.e., each dipole axis is parallel to the z-axis ($\theta_T = 0^\circ$), the electric field distribution in Fig. 3(b) shows the directly transmitted OAM waves in free space, with the array center at (0, 0, 3 m). Fig. 3(c) and (d) shows the distributions of the total electric field (maximum amplitude) with the reflected OAM waves originating from the image OAM array at (0, 0, -3 m). Four additional shadow regions of small amplitude (blue color) appear and split the electric field patterns. The radiation pattern in Fig. 4(a) demonstrates that those four shadow regions appear at $\theta = \pm 42^\circ$ and $\pm 76^\circ$.

For the case that the Tx array is rotated by 90° ($\theta_T = 90^\circ$), the electric field distributions change corresponding to Fig. 3(f)–(h). Twisting electric field distributions are visible in free space, as demonstrated in Fig. 3(f). Due to the presence of the ground plane, the electric fields in Fig. 3(g) and (h) are split as well. Unlike the vertical OAM array case in Fig. 3(c), the shadow region in Fig. 3(g) is not symmetric in the yz-plane. The radiation pattern in Fig. 4(b) reveals two shadow regions in the xz-plane at $\theta = \pm 38^\circ$.

The minima in electric field distributions and radiation patterns, respectively, are the direct effect of destructive interference between original and image OAM arrays. This effect is well known and was expected. However, it is hard to directly derive from this the performance of OAM-based communication. For example, Fig. 3(g) shows the electric field distribution is split whereby most field parts are still focused around the array center and twisting in phase.

III. OAM-Based Communication Above Infinite Ground Plane

In this section, the impact of both wave contributions, directly transmitted and reflected, will be studied by using the mixed-mode scattering parameters, which include information on all OAM modes. In order to compute the OAM-based communication between a transmitting array (Tx) and a receiving array (Rx), as illustrated in Fig. 1, each dipole is excited by a generator representing a port both at the Tx and the Rx arrays. Then a 16×16 standard scattering matrix $\mathbf{S}$ is obtained by full-wave simulations using MoM. With a specifically constructed unitary transformation matrix [21], a mixed-mode scattering matrix $\mathbf{M}$ in terms of OAM modes is derived from $\mathbf{S}$, that describes the

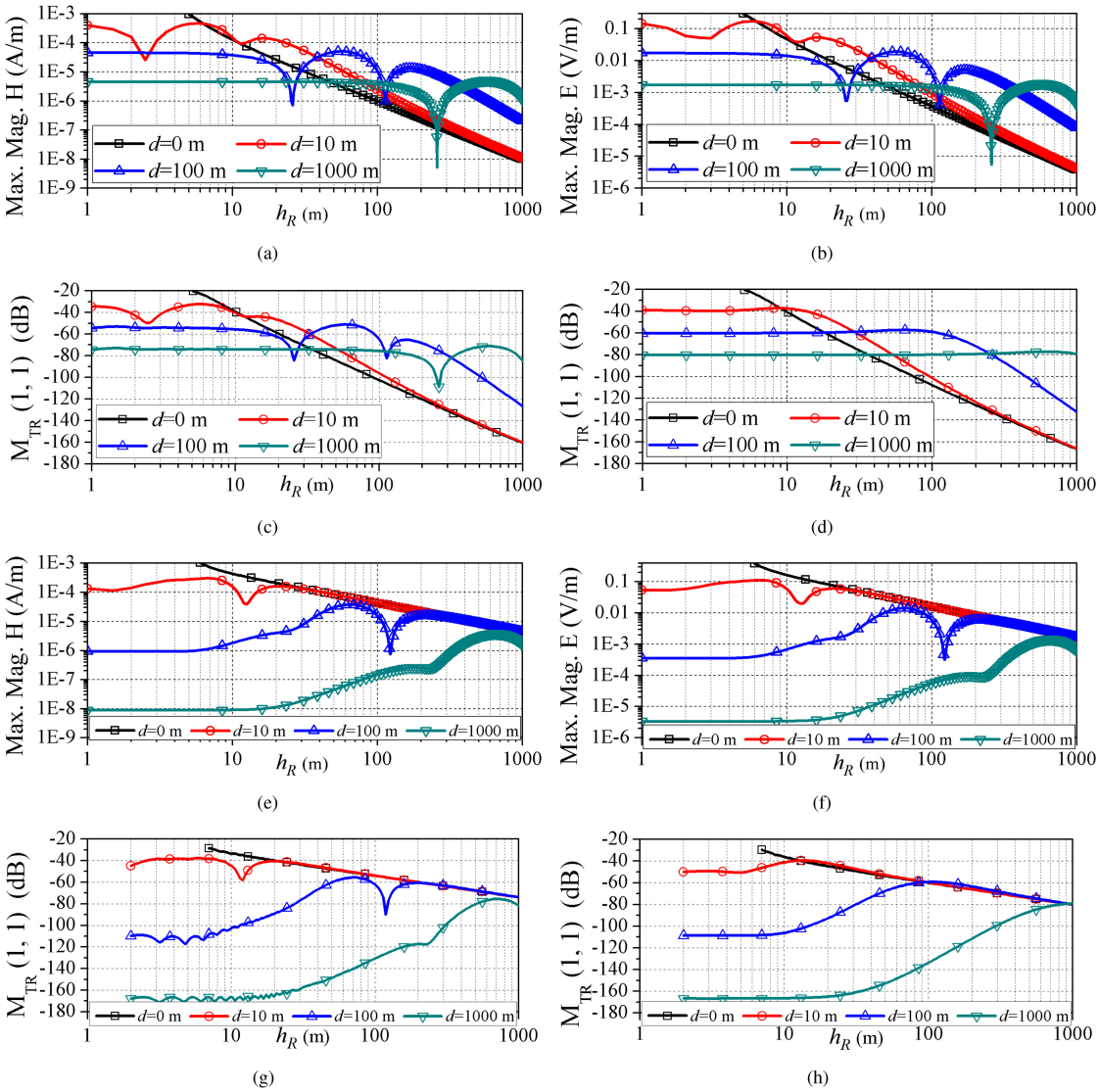

Fig. 5. Maximum magnitudes of EM fields and magnitudes of OAM communication $\mathbf{M_{tr}}(1, 1)$ due to the infinite ground effect, versus different communication distances d from 1 to 1000 m for $h_T = 3$ m. Values are obtained from full-wave simulation using MoM. (a)–(d): $\theta_T = \theta_R = 0°$; (e)–(h): $\theta_T = \theta_R = 90°$. (a) and (e) are the magnetic fields. (b) and (f) are the electric fields, whereas the others are the transmission mixed-mode scattering parameters of $\mathbf{M_{tr}}(1, 1)$ with [(c) and (g)] and without [(d) and (h)] ground plane.

OAM-based communication between Tx and Rx arrays, with respect to modes instead of generator ports.

A. Relation of OAM Communication and EM Fields

How the mentioned shadow regions in Fig. 3 affect the OAM communication will be discussed in this section. OAM waves of mode 1 are chosen to explore the communication between two OAM arrays.

The OAM communication for mode 1 of two vertical OAM arrays ($\theta_T = \theta_R = 0°$) with different distances $d = 0$, 10, 100, and 1000 m is demonstrated in Fig. 5(c). The Tx array is set to $h_T = 3$ m, which is the same height as applied in Fig. 3. Compared to the free space case as shown in Fig. 5(d), there are several positions h_R of minimum communication, such as at $h_R = 2.6$ m and $h_R = 11$ m if $d = 10$ m, $h_R = 26$ m and $h_R = 110$ m if $d = 100$ m, $h_R = 260$ m, and $h_R = 1100$ m if $d = 1000$ m. For each curve in Fig. 5(b), there are two minima, which agrees with the shadow regions of the electric field distributions in Fig. 3(d). The plot of the maximum magnitude of the EM fields in Fig. 5(a) and (b) confirms that the minima of OAM mode communication and of the EM fields are at the same positions (h_R). Closer inspection reveals that the minimum regions remain

TABLE I
DIRECT AND REFLECTED OAM MODE TRANSMISSION

Mixed-mode matrices	(1, 1)	(2, 1)	(3, 1)	(-1, 1)	(-2, 1)	(-3, 1)
$\mathbf{M_{tr_d}}$	-78.20	-201.17	-173.43	-185.89	-208.20	-170.08
$\mathbf{M_{tr_r}}$	-80.42	-96.47	-112.72	-76.48	-87.37	-99.86
$\mathbf{M_{tr}}$	-80.79	-89.98	-85.59	-78.30	-85.11	-85.73

OAM mode 1 is generated by the Tx array whereas mode ±1, ±2, and ±3 are received at the Rx array. ($h_T = h_R = 2$ m, $d = 30$ m, and $\theta_T = \theta_R = 90°$, values in dB).

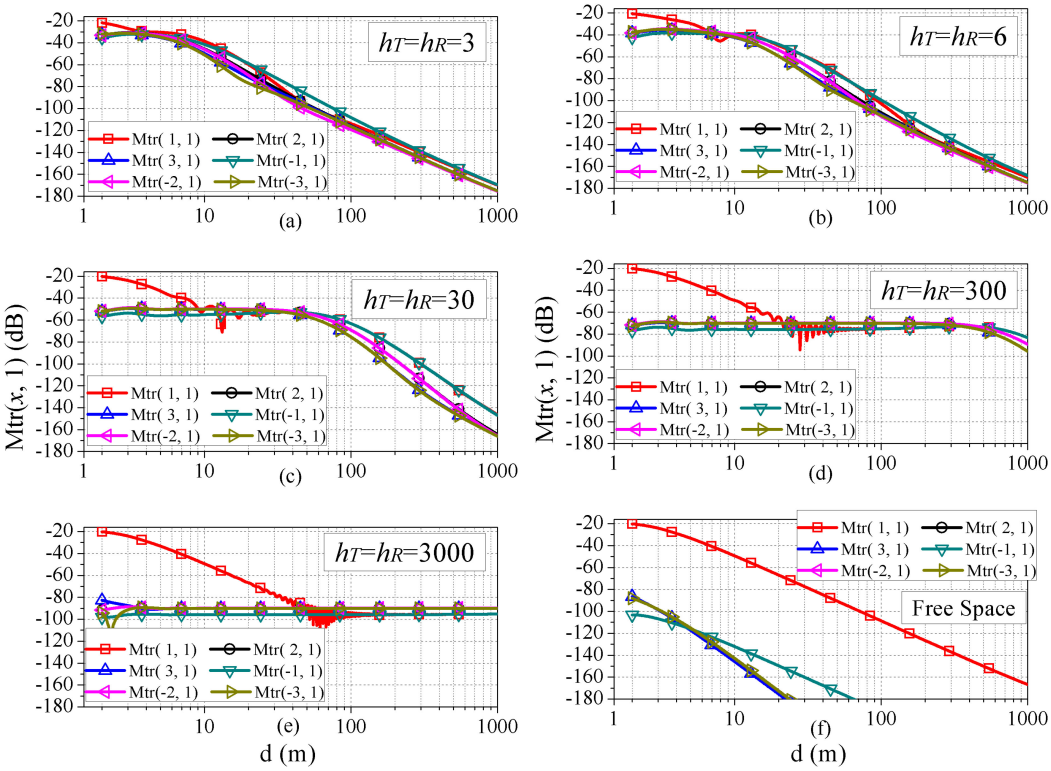

Fig. 6. Different received modes at Rx when an OAM wave of mode 1 is transmitted at Tx. Tx and Rx are coaxially arranged ($\theta_T = \theta_R = 90°$) at the same height above the ground. The height $h_T = h_R$ varies from 3, 6, 30, and 300–3000 m. The distance d between Tx and Rx is varying from 2 to 1000 m. Corresponding data in free space are added for reference.

at $\theta = 90° - \tan^{-1}(2.6/10) \approx 76°$ and $\theta = 90° - \tan^{-1}(11/10) \approx 42°$, which also agrees with the radiation pattern in Fig. 4(a).

In Fig. 5(g), the same situation for the minimum OAM communication is visible for the horizontal OAM array ($\theta_T = \theta_R = 90°$). The OAM communication and the magnitude of EM fields both have minima at $h_R = 13$ m for $d = 10$ m, $h_R = 130$ m for $d = 100$ m, and $h_R = 1300$ m for $d = 1000$ m. The corresponding angle θ is $\theta = 90° - \tan^{-1}(13/10) \approx 38°$, coinciding with the minimum positions predicted in Fig. 4(b).

It can be concluded that a minimum in the EM field leads to a minimum in the OAM communication of corresponding modes in all the cases investigated. However, the mode conversions of OAM waves between different topology charges cannot be derived from the EM fields. So, we cannot make any conclusions on the OAM communication between different modes. In the future, the investigation has to be extended to the interference on general OAM-based communication.

B. Contributions of Direct and Reflected OAM Communication

Corresponding to the analysis in Section II-A, OAM waves above ground can be separated into a directly transmitted contribution and a reflected contribution due to the influence of the ideal ground plane. The reflected part can be represented by an image OAM array. In the following, by using MoM and mixed-mode scattering parameters, the received OAM wave of mode k from the reflection is computed by calculating the transmission $\mathbf{M_{tr_r}}(k, i)$ from the image OAM array Tx′ to the observation OAM array Rx, when the mode i wave is transmitted, where $k, i = \pm1, \pm2, \pm3$ for an eight dipole OAM array. In addition, $\mathbf{M_{tr_d}}(k, i)$ is the direct transmission from the OAM array Tx to the observation Rx array, and $\mathbf{M_{tr}}(k, i)$ is the total transmission from the Tx array to the Rx array, including the impact of an infinite ground, which is a combination of the direct transmission from Tx and the reflection from ground. The Tx and Rx arrays are oriented both in x direction ($\theta_T = \theta_R = 90°$) and coaxially located at the same height ($h_T = h_R = 2$ m) above the ground. The Rx array is $d = 30$ m away from the Tx array.

As shown in Table I, the direct transmission $\mathbf{M_{tr_d}}(1, 1)$ is more than 90 dB higher than other modes when mode 1 is transmitted by the Tx array. As a result, the transmitted mode can be distinguished from all the received OAM modes at the Rx array. The received OAM wave from reflection $\mathbf{M_{tr_r}}(-1, 1)$ is higher in amplitude than $\mathbf{M_{tr_r}}(1, 1)$ according to Table I. The latter value is at the same power level as the direct transmission $\mathbf{M_{tr_d}}(1, 1)$ is. When the direct transmission and the reflection are combined to the total communication, the received $\mathbf{M_{tr}}(-1, 1)$ is -78.30 dB, even higher than $\mathbf{M_{tr}}(1, 1) = -80.79$ dB.

As a result, the highest received mode at Rx is the mode -1, whereas the transmitted mode at Tx is the mode 1. Hence, the transmitted OAM modes cannot be distinguished at the Rx due to the infinite ground effect.

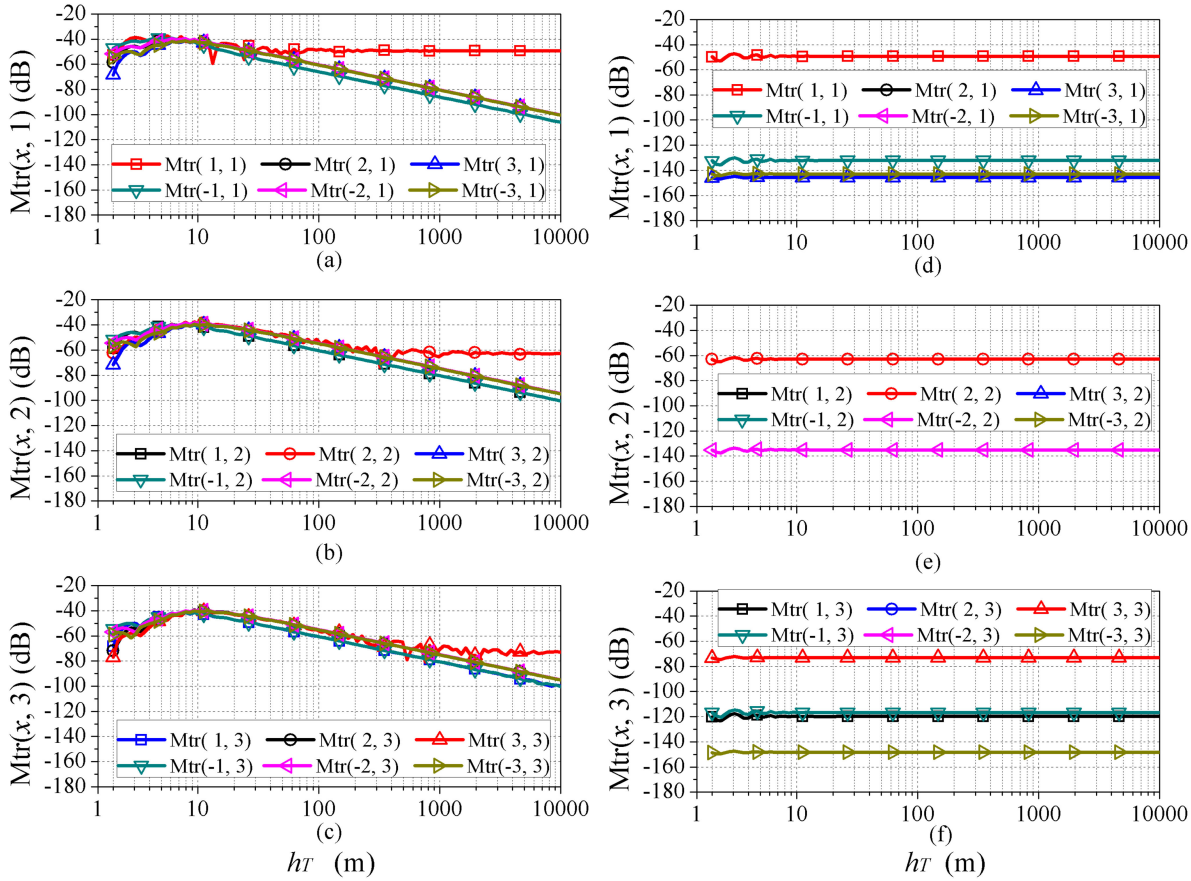

Fig. 7. OAM-based communication system of two OAM arrays with an infinite ground plane. (a)–(c) $\theta_T = \theta_R = 90°$ and $h_R = h_T$. (d)–(f) $\theta_T = \theta_R = 0°$ and $h_R = h_T$ + 10 m.

C. OAM Communication at Different Distances

The total OAM communication, $\mathbf{M_{tr}}$ in Table I shows that the mode of the transmitted OAM wave from the Tx array cannot be detected at Rx array due to the ground effect. In this section, it will explore whether this phenomenon is present for all communication distances d between the Tx and Rx arrays.

OAM communication, as a function of distance d between both arrays, was studied [18] in free space without a ground plane. The study in Table I summarizes the OAM mode communication at a fixed distance $d = 30$ m with a ground plane being present. As an extension to this, Fig. 6 depicts the infinite ground effect versus different communication distances. It is noted in [21] that when the Tx and Rx arrays are coaxially arranged and face-to-face located, the transmitted mode has the largest isolation to the other modes. Hence, Tx and Rx are coaxially aligned and located at the same height $h_T = h_R$ here. For comparison, the corresponding results in free space are also included in Fig. 6. Different heights h_T vary from 3, 6, 30, and 300–3000 m.

Analyzing the curves in Fig. 6, the following can be concluded: when $h_T = h_R = 3$ m, the mode isolation at $d = 2$ m is 10 dB and all the modes are "mixed" (showing the same amplitude) when d is getting larger than 4 m. At the height $h_T = h_R = 6$ m, the mode isolation for the array distance $d =$ 2 m is 18 dB and all OAM modes are mixed for $d > 6$ m. When considering $h_T = h_R = 30$ m, the mode isolation at $d = 2$ m is 30 dB and all modes are mixed for $d > 9$ m. Given $h_T = h_R =$ 300 m, the mode isolation at $d = 2$ m is 50 dB and all modes are mixed for $d > 20$ m. In the case of $h_T = h_R = 3000$ m, the mode isolation at $d = 2$ m is 60 dB and all the modes are mixed after $d > 40$ m.

It is found that the relative mode isolation increases when the Tx and Rx arrays move away from the ground. Moreover, the maximum distance that the dominant mode (transmitted by the Tx) can be distinguished at Rx extends with increasing array heights. A "mode distinguishable" region is defined from 2 m to the maximum distance that $\mathbf{M_{tr}}(1, 1)$ is still the highest in amplitude that can be distinguished. Comparing to the free-space case, in the distinguishable region, $\mathbf{M_{tr}}(1, 1)$ keeps the same value as in free space, but the received noise modes, which are represented by $\mathbf{M_{tr}}(x, 1)$, $x \neq 1$, increase in amplitude. In other words, the infinite ground does not affect the dominant mode communication, but increases the received noise modes ($\mathbf{M_{tr}}(x, 1)$) in the mode distinguishable region.

D. OAM Communication at Different Heights

So far, the article only investigated the OAM-based communication at four heights $h_T = h_R$ of 3, 6, 30, 300, and 3000 m.

In this section, a possible height effect on the communication between two OAM arrays shall be explored.

In Fig. 7(a), two horizontal OAM arrays ($\theta_T = \theta_R = 90^\circ$) are in a coaxial setup with a fixed distance of $d = 10$ m. The indicated height h_T ($h_R = h_T$) over the ground varies from 2 m to 10 km. Fig. 7(a) shows that the OAM communication $\mathbf{M_{tr}}(1, 1)$ becomes dominant in the received modes when the height is more than 50 m. The same can be found for $\mathbf{M_{tr}}(2, 2)$ when $h_T > 400$ m, and $\mathbf{M_{tr}}(3, 3)$ when $h_T > 1000$ m. Moreover, the dominant mode communication $\mathbf{M_{tr}}(1, 1)$, (2, 2), and (3, 3) remain constant in the distinguishable regions, i.e., from 50 to 10 km for $\mathbf{M_{tr}}(1, 1)$. Another investigation is carried out by shifting the OAM arrays along the $\hat{e}_z$ direction, as shown in Fig. 7(d)–(f), where $\theta_T = \theta_R = 0^\circ$. Again the OAM mode communication is investigated as a function of the height h_T, where $h_R = h_T$ + 10 m to maintain a fixed communication distance $d = 10$ m. The dominant mode communication $\mathbf{M_{tr}}(1, 1)$, (2, 2), and (3, 3) remain the same as in the free-space case, as shown in Fig. 7(d)–(f), only with a tiny difference of trivial variations when height h_T is very close to the ground ($h_T < 5$ m).

Fig. 7 indicates that the infinite ground mixes all the received OAM modes when the horizontal OAM arrays are lower than 10λ to the ground. But when the arrays are higher than 400λ, the dominant OAM mode communication will be detected at Rx again. For different OAM mode communication such heights are different. Typically higher OAM modes need larger heights above the ground to be detected in the mix of all OAM modes. However, the infinite ground does not affect the vertical OAM communication system, which is similar to the communication of two vertical dipoles above a ground plane.

IV. Conclusion

The impact of an infinite ground plane on OAM-based communication has been investigated in this article. Radiation patterns in terms of electric field amplitudes can be used to find the minimum and maximum communication angles for individual OAM modes, which might be useful for the purpose of interference reduction or antijamming. Several two-array communication systems covering different OAM modes have been explored. The results imply that an infinite ground plane has a strong impact on the wireless communication between two OAM arrays. The communication of an individual mode is increased when the OAM arrays are close to the ground plane and then decreased to a constant value when assuming larger heights. When two OAM arrays are close to each other, the transmitted mode will be received at the same power level as in the case of free space and can still be distinguished at the receiver. But the amplitude of other "noise" modes increases, which will reduce the signal-to-noise ratio. The ground plane mixes the received modes at the OAM receiver when the two arrays are more than 6λ away from each other and 100λ above a ground plane. This makes the transmitted OAM mode difficult to detect. Such an effect will fade when the OAM arrays are at, e.g., 1000λ above the ground plane. The fading effect varies depending on the different OAM modes. In addition, it is found that the ground effect is influenced by the array orientations.

Acknowledgment

Dr. L. Wang would like to thank Alexander von Humboldt Foundation for the support of his research stay in Germany.

References

[1] R. Gaffoglio, A. Cagliero, G. Vecchi, and F. P. Andriulli, "Vortex waves and channel capacity: Hopes and reality," *IEEE Access*, vol. 6, pp. 19 814–19 822, 2018.

[2] A. E. Willner, "Communication with a twist," *IEEE Spectrum*, vol. 53, no. 8, pp. 34–39, Aug. 2016.

[3] G. Gibson *et al.*, "Free-space information transfer using light beams carrying orbital angular momentum," *Opt. Express*, vol. 12, no. 22, pp. 5448–5456, Nov. 2004.

[4] F. Tamburini, E. Mari, A. Sponselli, B. Thidé, A. Bianchini, and F. Romanato, "Encoding many channels on the same frequency through radio vorticity: First experimental test," *New J. Phys.*, vol. 14, no. 3, Mar. 2012, Art. no 033001.

[5] A. E. Willner *et al.*, "Design challenges and guidelines for free-space optical communication links using orbital-angular-momentum multiplexing of multiple beams," *J. Opt.*, vol. 18, no. 7, Jun. 2016, Art. no 074014.

[6] B. Thide *et al.*, "Utilization of photon orbital angular momentum in the low-frequency radio domain," *Phys. Rev. Lett.*, vol. 99, Aug. 2007, Art. no 087701.

[7] S. M. Mohammadi *et al.*, "Orbital angular momentum in radio: Measurement methods," *Radio Sci.*, vol. 45, no. 4, pp. 1–14, Aug. 2010.

[8] K. Murata, N. Honma, K. Nishimori, N. Michishita, and H. Morishita, "Analog eigenmode transmission for short-range MIMO based on orbital angular momentum," *IEEE Trans. Antennas Propag.*, vol. 65, no. 12, pp. 6687–6702, Dec. 2017.

[9] M. Lin, Y. Gao, P. Liu, and J. Liu, "Theoretical analyses and design of circular array to generate orbital angular momentum," *IEEE Trans. Antennas Propag.*, vol. 65, no. 7, pp. 3510–3519, Jul. 2017.

[10] A. Cagliero, "Symmetry breaking in UCA-based vortex waves," *J. Phys. Commun.*, vol. 2, no. 9, Sep. 2018, Art. no 095012.

[11] W. Park, D. G. Kam, H. Brüns, and C. Schuster, "Numerical investigation of orbital angular momentum density of antenna arrays based on the method of moments," in *Proc. IEEE Int. Symp. Electromagn. Compat. IEEE Asia-Pacific Symp. Electromagn. Compat.*, May 2018, pp. 88–93.

[12] S. M. Mohammadi *et al.*, "Orbital angular momentum in radio–A system study," *IEEE Trans. Antennas Propag.*, vol. 58, no. 2, pp. 565–572, Feb. 2010.

[13] O. Edfors and A. J. Johansson, "Is orbital angular momentum (OAM) based radio communication an unexploited area?" *IEEE Trans. Antennas Propag.*, vol. 60, no. 2, pp. 1126–1131, Feb. 2012.

[14] K. A. Opare, Y. Kuang, and J. J. Kponyo, "Mode combination in an ideal wireless OAM-MIMO multiplexing system," *IEEE Wireless Commun. Lett.*, vol. 4, no. 4, pp. 449–452, Aug. 2015.

[15] X. Chen, W. Xue, H. Shi, J. Yi, and W. E. I. Sha, "Orbital angular momentum multiplexing in highly reverberant environments," *IEEE Microw. Wireless Compon. Lett.*, vol. 30, no. 1, pp. 112–115, Jan. 2020.

[16] X. Gao *et al.*, "An orbital angular momentum radio communication system optimized by intensity controlled masks effectively: Theoretical design and experimental verification," *Appl. Phys. Lett.*, vol. 105, no. 24, 2014, Art. no 241109.

[17] K. Liu, Y. Cheng, Y. Gao, X. Li, Y. Qin, and H. Wang, "Super-resolution radar imaging based on experimental OAM beams," *Appl. Phys. Lett.*, vol. 110, no. 16, 2017, Art. no 164102.

[18] D. K. Nguyen, O. Pascal, J. Sokoloff, A. Chabory, B. Palacin, and N. Capet, "Antenna gain and link budget for waves carrying orbital angular momentum," *Radio Sci.*, vol. 50, no. 11, pp. 1165–1175, 2015.

[19] A. Cagliero, A. D. Vita, R. Gaffoglio, and B. Sacco, "A new approach to the link budget concept for an OAM communication link," *IEEE Antennas Wireless Propag. Lett.*, vol. 15, pp. 568–571, 2016.

[20] Y. Yao, X. Liang, M. Zhu, W. Zhu, J. Geng, and R. Jin, "Analysis and experiments on reflection and refraction of orbital angular momentum waves," *IEEE Trans. Antennas Propag.*, vol. 67, no. 4, pp. 2085–2094, Apr. 2019.

[21] W. Park, L. Wang, H. Brüns, D. G. Kam, and C. Schuster, "Introducing a mixed-mode matrix for investigation of wireless communication related to orbital angular momentum," *IEEE Trans. Antennas Propag.*, vol. 67, no. 3, pp. 1719–1728, Mar. 2019.

[22] L. Wang, W. Park, H. Brüns, D. G. Kam, and C. Schuster, "Numerical investigation of the impact of array orientations on orbital angular momentum (OAM) based communication using a mixed-mode matrix," in *Proc. 12th German Microw. Conf.*, Mar. 2019, pp. 55–58.
[23] L. Wang, C. Yang, H. Brüns, and C. Schuster, "Effect of the interference from conducting plates on OAM based wireless communication," in *Proc. Int. Conf. Electromagn. Adv. Appl.*, Sep. 2019, pp. 0803–0806.
[24] W. L. Stutzman and G. A. Thiele, *Antenna Theory and Design*. New York, NY, USA, Wiley, 1981.
[25] Hamburg University of Technology (TUHH), Hamburg, Germany. CONCEPT-II. [Online]. Available: http://www.tet.tuhh.de/concept/, Accessed on: Oct. 2019.
[26] C. Su and T. K. Sarkar, "Adaptive multiscale moment method (AMMM) for analysis of scattering from perfectly conducting plates," *IEEE Trans. Antennas Propag.*, vol. 48, no. 6, pp. 932–939, Jun. 2000.

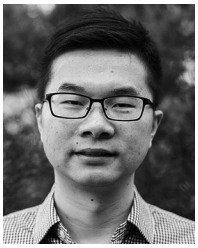

Lei Wang (Senior Member, IEEE) received the Ph.D. degree in electromagnetic field and microwave technology from Southeast University, Nanjing, China, in 2015.

From 2014 to 2016, he was a Research Fellow and Postdoc with the Laboratory of Electromagnetics and Antennas, Swiss Federal Institute of Technology, Lausanne, Switzerland. From October 2016 to November 2017, he was a Postdoc Research Fellow with the Electromagnetic Engineering Laboratory, KTH Royal Institute of Technology, Stockholm, Sweden. Since November 2017, he is an Alexander von Humboldt Fellow with the Institute of Electromagnetic Theory of Hamburg University of Technology, Hamburg, Germany. His research interests include the antenna theory and applications, active electronically scanning arrays, integrated antennas and arrays, substrate-integrated waveguide antennas, leaky-wave antennas, and wireless propagation.

Dr. Wang was the recipient of the Chinese National Scholarship for Ph.D. Candidates and was also granted the Swiss Government Excellence Scholarship to conduct research on SIW horn antennas and applications in 2014. In 2016, he was granted by the Alexander von Humboldt Research Foundation to take research on antenna modeling and optimization. Moreover, he was a recipient of the Best Poster Award in 2018 IEEE International Workshop on Antenna Technology (iWAT).

Woocheon Park received the B.S., M.S., and Ph.D. degrees in electrical engineering from Ajou University, Suwon, South Korea, in 2013, 2015, and 2019, respectively.

From 2017 to 2018, he was a Visiting Researcher with the Institute of Electromagnetic Theory, Hamburg University of Technology, Hamburg, Germany. Since 2019, he has been with the Electronics and Telecommunications Research Institute, Daejeon, South Korea. His research interests include numerical electromagnetics, EMI/EMC, antenna applications, and electromagnetic communications.

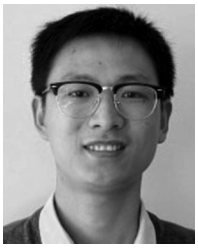

Cheng Yang (Member, IEEE) received the B.S. degree in electronic science and technology from Wuhan University, Wuhan, China, in 2009, and the M.S. and Ph.D. degrees in electromagnetic field and microwave technology from the National University of Defense Technology, Changsha, China, in 2012 and 2016, respectively.

Since 2019, he has been a Senior Engineer with the Institute of Electromagnetic Theory, Technische Universität Hamburg (TUHH), Hamburg, Germany. From 2013 to 2015, he was funded a Joint Ph.D. Student with TUHH by the Chinese Scholarship Councilas. From 2016 to 2019, he was a Faculty Member with the State Key Laboratory of Millimeter Wave at Southeast University, Nanjing, China. His research interests include computational electromagnetics, microwave measurement techniques, design and analysis of nonlinearly loaded electromagnetic structures.

Heinz-Dietrich Brüns was born in Bremerhaven, Germany, in 1953. He received the Diploma from the Technische Universität Braunschweig, Brunswick, Germany, in 1980, and the Ph.D. degree from the Universität der Bundeswehr, Hamburg, Germany, in 1985, both in electrical engineering.

He has been with the Hamburg University of Technology, Hamburg, since 1985. His research interests include the method of moments and numerical techniques in electromagnetics.

Dong Gun Kam (Senior Member, IEEE) received the B.S. degree in physics with a double major in electrical engineering, and the M.S. and Ph.D. degrees in electrical engineering from KAIST, Daejeon, South Korea, in 2000, 2002 and 2006, respectively.

From 2007 to 2011, he was with the IBM Watson Research Center, Yorktown Heights, NY, USA, concentrating on the subsystem design and analysis of high-speed wireline and wireless links. In 2011, he joined Ajou University, Suwon, South Korea. His research interests include millimeter-wave antennas and packages and EMI/EMC. He is currently on sabbatical leave at NC State University, as a Visiting Associate Professor.

Dr. Kam is currently an Associate Editor for the IEEE TRANSACTIONS ON COMPONENTS, PACKAGING AND MANUFACTURING TECHNOLOGY. He was a recipient of the 2008 DesignCon Paper Award; a recipient of the 2011 Pat Goldberg Memorial Award for the Best Paper in CS, EE, and Math within IBM Research; and a recipient of the 2013 CPMT Outstanding Young Engineer Award.

Christian Schuster (Senior Member, IEEE) received the Diploma in physics from the University of Konstanz, Germany, in 1996, and the Ph.D. degree in electrical engineering from the Swiss Federal Institute of Technology, Zurich, Switzerland, in 2000.

Since 2006, he has been a Full Professor and Head of the Institute of Electromagnetic Theory with the Hamburg University of Technology, Hamburg, Germany. Prior to that, he was with the IBM T. J. Watson Research Center, Yorktown Heights, NY, USA, where he was involved in high-speed optoelectronic package and backplane interconnect modeling and signal integrity design for new server generations. His research interests include signal and power integrity of digital systems, multiport measurement and calibration techniques, and development of electromagnetic simulation methods for communication electronics.

Dr. Schuster was a recipient of the IEEE TRANSACTIONS ON ELECTROMAGNETIC COMPATIBILITY Best Paper Awards in 2001 and 2015, IEEE TRANSACTIONS ON COMPONENTS, PACKAGING AND MANUFACTURING TECHNOLOGY Best Paper Awards in 2012 and 2016, IEC DesignCon Paper Awards in 2005, 2006, 2010, 2017, and 2018, three IBM Research Division Awards between 2003 and 2005, and IBM Faculty Awards in 2009 and 2010. Also, in 2019, he received the Sustained Service to the EMC Society Award. He is a member of the German Physical Society (DPG) and several technical program committees of international conferences on signal and power integrity, and electromagnetic compatibility. He was serving as a Distinguished Lecturer for the IEEE EMC Society from 2012 to 2103, as the Chair of the German IEEE EMC Chapter from 2016 to 2019, and is currently an Associate Editor for the IEEE TRANSACTIONS ON EMC and a member of the Board of Directors of the EMC Society.